

# Optimal colliding energy for the synthesis of superheavy element $Z=119$

Avazbek Nasirov<sup>1,2,\*</sup> and Bakhodir Kayumov<sup>3,2,†</sup>

<sup>1</sup>*Joint Institute for Nuclear Research, Dubna 141980, Russia*

<sup>2</sup>*Institute of Nuclear Physics, Tashkent 100214, Uzbekistan*

<sup>3</sup>*School of Humanities and Natural Sciences, New Uzbekistan University, Tashkent 100007, Uzbekistan*

The evaporation residue (ER) cross section of 3n and 4n channels related to the synthesis of superheavy element (SHE) with the charge number  $Z = 119$  in the  $^{51}\text{V} + ^{248}\text{Cm}$  reaction has been calculated by the dinuclear system (DNS) model as a sum of the partial cross sections of the corresponding channels. The angular momentum distribution of the compound nucleus is estimated by the dynamical trajectory calculations of the capture probability which is considered as the DNS formation probability. The fusion probability decreases by the increase of the DNS angular momentum due to its influence on the intrinsic fusion barrier  $B_{\text{fus}}^*$ . The range  $\alpha_2 = 60^\circ \div 70^\circ$  of the orientation angle of the axial symmetry axis of the deformed target nucleus  $^{248}\text{Cm}$  is favorable for the formation of the compound nucleus. The fusion probability decreases at around  $\alpha_2 = 90^\circ$  since the number of the partial waves contributing to the capture decreases. Therefore, it is important to calculate the capture cross section dynamically. The 4n channel cross section of the SHE synthesis is larger than the 3n channel cross section maximum value of the ER cross section is 12.3 fb at  $E_{c.m.} = 232$  MeV.

## I. INTRODUCTION

The synthesis of superheavy elements (SHE) represents a remarkable achievement in the field of nuclear physics [1]. These exotic elements, characterized by staggering atomic masses and short lifetime, have intrigued scientists for decades. The heaviest superheavy element which was synthesized by using  $^{48}\text{Ca}$ -induced complete fusion reactions have been successfully used to synthesize SHE with charge numbers  $Z = 112$ – $118$  in the neutron evaporation channels [2–8]. However, reactions  $^{50}\text{Ti} + ^{249}\text{Bk}$  and  $^{249}\text{Cf}$  [9],  $^{54}\text{Cr} + ^{248}\text{Cm}$  [10] and  $^{58}\text{Fe} + ^{244}\text{Pu}$  [11] did not provide success for the synthesis of SHEs with  $Z = 119$  and 120.

A lot of theoretical investigations devoted to describing the measured data of the evaporation residue cross sections and to making predictions for their values in the different reactions leading to the formation of the SHE with  $Z = 119$  and 120 have been done [12–18]. Their results can be useful to make a choice of a pair of colliding nuclei and to fix a range of the beam energies leading to the observable cross sections in the synthesis of the wanted SHE. The authors in Ref. [13] made a conclusion that the most promising reactions of the synthesis of superheavy elements  $Z = 119$  and  $Z = 120$  are  $^{50}\text{Ti} + ^{248}\text{Bk}$  and  $^{50}\text{Ti} + ^{249,251}\text{Cf}$ , respectively. However, in Ref. [12] the maximum values of the ER cross section in the  $^{50}\text{Ti} + ^{249}\text{Bk}$  and  $^{51}\text{V} + ^{248}\text{Cm}$  reactions 0.064 pb and 0.01 pb were obtained for the 4n channel.

The very small cross sections obtained in the synthesis of SHE require finding favorable reactions (projectile and target pair) and the optimal beam energy range which is very narrow (no more than 10 MeV). The evaporation residue (ER) formation process is the last stage of the

complicated reaction mechanism in heavy-ion collisions near the Coulomb barrier energies. The whole process of the synthesis can be divided into three steps.

1. The first stage is a competition between deep-inelastic collision (incomplete momentum transfer) and the capture process (full momentum transfer). As a function of the initial collision energy and impact parameter, one of the above-mentioned two events takes place. If after dissipation of the sufficient part of the relative kinetic energy the system is able to overcome the Coulomb barrier from the inside to outside the deep-inelastic collision occurs (see Fig.1 in Ref. [19]) and if the residual part of the kinetic energy is not enough to overcome the Coulomb barrier the system is trapped into the potential well of the nucleus-nucleus interaction (see Fig. 2 in Ref. [20]). The last case is called capture and full momentum transfer of the relative motion to the shape and intrinsic degrees of freedom takes place. The difference between the lifetimes of the dinuclear system (DNS) formed at capture and deep-inelastic collisions depends on whether the path of relative motion has been trapped into the potential well or not. The lifetime of the DNS formed at capture is longer in comparison to the one of DNS formed in the deep-inelastic collisions. This competition strongly depends on the collision energy and the impact parameter (angular momentum of relative motion). The range of the angular momentum of the compound nucleus (CN) is established in the capture stage.
2. In the subsequent stage of the reaction, the evolution of the DNS goes in two possible outcomes: the formation of a compound nucleus (CN) in an equilibrium state with an excitation energy denoted as  $E_{\text{CN}}^*$ , or DNS may break up in two distinct fragments without reaching the state of CN. The latter process is called as quasifission. The quasifis-

\* nasirov@jinr.ru

† b.kayumov@newuu.uz

sion occurs when the DNS prefers to break up into two fragments rather than transforming into a fully equilibrated CN. The quasifission is the main hindrance to the CN formation during the evolution of DNS in reactions with massive nuclei, since this process is dominant in comparison to the complete fusion.

3. The third stage of the process involves the formation of a rotationally excited mononucleus, which occurs due to a phenomenon driven by the transfer of all nucleons from the lighter fragment to the heavier nucleus. The rotation of this non-equilibrium mononucleus leads to a reduction in the fission barrier, as discussed in Ref. [21]. Consequently, at a specific value of the orbital angular momentum, the fission barrier vanishes entirely. In such a scenario, the non-equilibrium mononucleus becomes inherently unstable and undergoes fission. The splitting of a mononucleus before reaching its equilibrium state is called fast-fission, as a result of which binary mass-symmetric fragments are formed.

Finally, the CN, which survives fission during its cooling by the emission of neutrons, protons, alpha particles, and gamma quanta forms the ER. The result of this competition is estimated by the survival probability  $W_{\text{sur}}$ . According to all these stages, ER cross section  $\sigma_{\text{ER}}$  can be calculated as summation over all partial waves  $\ell$  as described in references [22, 23]:

$$\sigma_{\text{ER}}(E_{\text{c.m.}}) = \sum_{\ell} \sigma_{\text{cap}}(E_{\text{c.m.}}, \ell) P_{\text{CN}}(E_{\text{c.m.}}, \ell) \times W_{\text{sur}}(E_{\text{c.m.}}, \ell) \quad (1)$$

The short description of the model used in calculation of the cross sections of the capture, complete fusion and ER formation in competition with the fission is presented in Section II. The results of calculation of the partial fusion and quasifission cross sections are discussed in Section III.

## II. MODEL

### A. Capture cross section

Two conditions must be satisfied for the capture:

- 1) The initial energy  $E_{\text{c.m.}}$  of a projectile in the center-of-mass system should be larger than the minimum of the potential well of the nucleus-nucleus interaction (Coulomb barrier + rotational energy of the entrance channel) to overcome or by tunneling through the barrier along relative distance in the entrance channel to form a DNS;
- 2) At the same time the value of the relative kinetic energy above the entrance channel barrier should be in correspondence with the size of the potential well: in case of the collision of the massive nuclei the size of the potential is small and, if the initial collision energy is very large relative to the entrance channel barrier, the dissipation of the kinetic energy maybe not enough to make its value lower than a barrier of potential well, i.e. to cause trapping into potential well. As a result, the capture does not occur and the deep-inelastic collision takes place. These events are separated by the analysis of the collision dynamics. The range of the values of the orbital angular momentum leading to capture is determined by solving the equations of motion for the relative distance  $R$  and orbital angular momentum  $\ell$  [20, 24]. Trajectory calculations show that the values of  $\ell$  leading to capture can form a "window".

Theoretical values of the capture cross sections are calculated with the quantities characterizing the entrance channel by the formula [19]:

$$\sigma_{\text{cap}}(E_{\text{c.m.}}, \ell; \{\alpha_i, \beta_i\}) = \frac{\lambda^2}{4\pi} (2\ell + 1) \times \mathcal{P}_{\text{cap}}^{\ell}(E_{\text{c.m.}}, \ell; \{\alpha_i, \beta_i\}), \quad (2)$$

where  $\lambda$  is the de Broglie wavelength of the entrance channel and  $\mathcal{P}_{\text{cap}}^{\ell}(E_{\text{c.m.}}, \ell; \{\alpha_i, \beta_i\})$  is the capture probability;  $\{\beta_i\}$  are parameters of the shape deformation of the colliding nuclei "1" and "2";  $\alpha_i$  are orientation angles of the axial symmetry axis of the colliding nuclei relative to the beam.

$$\mathcal{P}_{\text{cap}}^{(\ell)}(E_{\text{c.m.}}, \ell, \{\alpha_i, \beta_i\}) = \begin{cases} 1, & \text{if } \ell_m < \ell < \ell_d \text{ and } E_{\text{c.m.}} > V_B, \\ 0, & \text{if } \ell < \ell_m \text{ or } \ell > \ell_d \text{ and } E_{\text{c.m.}} > V_B \\ \mathcal{P}_{\text{tun}}^{(\ell)}(E_{\text{c.m.}}, \ell, \{\alpha_i, \beta_i\}), & \text{for all } \ell \text{ if } V_{\text{min}} < E_{\text{c.m.}} \leq V_B \end{cases} \quad (3)$$

where  $V_B$  and  $V_{\text{min}}$  are the barrier and minimum values of the potential well of the nucleus-nucleus interaction in the entrance channel;  $\ell_m$  and  $\ell_d$  are the minimum and maximum values of the orbital angular momentum  $\ell$  leading to capture at the given collision energy. The

boundary values  $\ell_m$  and  $\ell_d$  of the  $\ell$ -"window" leading to capture depend on the beam energy, the size of the potential well of the nuclear-nuclear potential, and the friction coefficients of radial motion and angular momentum.  $\mathcal{P}_{\text{tun}}^{(\ell)}$  is the probability of the barrier penetrability

which is calculated by the improved WKB formula by Kemble [25]:

$$\mathcal{P}_{tun}^{(\ell)}(E_{c.m.}, \{\alpha_i, \beta_i\}) = \frac{1}{1 + \exp[2K(E_{c.m.}, \ell, \{\alpha_i, \beta_i\})]}, \quad (4)$$

where

$$K(E_{c.m.}, \ell, \{\alpha_i, \beta_i\}) = \int_{R_{in}}^{R_{out}} dR \times \sqrt{\frac{2\mu}{\hbar^2} (V(R, \ell, \{\alpha_i, \beta_i\}) - E_{c.m.})}. \quad (5)$$

$R_{in}$  and  $R_{out}$  are inner and outer turning points which were estimated by  $V(R) = E_{c.m.}$ .

## B. Fusion cross section

The partial fusion cross section is determined by the product of capture cross section  $\sigma_{cap}(E_{c.m.}, \ell, \{\alpha_i, \beta_i\})$  and the fusion probability  $P_{CN}(E_{c.m.}, \ell, \{\alpha_i, \beta_i\})$  of DNS for the various excitation energies [26, 27]:

$$\sigma_{fus}(E_{c.m.}, \ell; \{\alpha_i, \beta_i\}) = \sigma_{cap}(E_{c.m.}, \ell; \{\alpha_i, \beta_i\}) \times P_{CN}(E_{c.m.}, \ell; \{\alpha_i, \beta_i\}), \quad (6)$$

In calculation of the fusion probability the change of the mass and charge distributions  $D_Z$  in the DNS fragments during capture is included [19], *i.e.* the fusion probability of the colliding nuclei is taken as a sum of the competition of complete fusion and quasifission at different charge asymmetry from the symmetric configuration  $Z_{sym}$  of DNS up to configuration corresponding to the maximum value of the driving potential  $Z_{max}$ :

$$P_{CN}(E_{c.m.}, \ell, \{\alpha_i, \beta_i\}) = \sum_{Z_{sym}}^{Z_{max}} D_Z(E_Z^*, \ell, \{\alpha_i, \beta_i\}) \times P_{CN}^{(Z)}(E_Z^*, \ell, \{\alpha_i, \beta_i\}). \quad (7)$$

The values of the  $D_Z(E_Z^*, \ell, \{\alpha_i, \beta_i\})$  are calculated by the solution of the transport master equation with the nucleon transition coefficients depending on the occupation numbers and energies of the single-particle states of nucleons of the DNS nuclei [19]. The fusion probability  $P_{CN}^{(Z)}(E_Z^*, \ell, \{\alpha_i, \beta_i\})$  for the DNS fragments with the charge configuration  $Z$  rotating with the orbital angular momentum  $\ell$  is calculated as the branching ratio of width  $\Gamma_{(fus)}^{(Z)}$  related to the sum of the widths overflowing over the quasifission barrier  $B_{qf}^Z(\alpha_i, \beta_i)$  at a given mass asymmetry, over the intrinsic barrier  $B_{fus}^{*(Z)}(\alpha_i, \beta_i)$  and symmetry barrier  $B_{sym}^{(Z)}(\alpha_i, \beta_i)$  on mass asymmetry axis [28]:

$$P_{CN}^{(Z)}(E_Z^*, B_{fus}^{*(Z)}, B_{qf}^{(Z)}, \ell) \approx \frac{\Gamma_{fus}^{(Z)}(B_{fus}^{*(Z)}, E_Z^*, \ell)}{\Gamma_{(qf)}^{(Z)}(B_{qf}^{(Z)}, E_Z^*, \ell) + \Gamma_{(fus)}^{(Z)}(B_{fus}^{*(Z)}, E_Z^*, \ell) + \Gamma_{sym}^{(Z)}(B_{sym}^{(Z)}, E_Z^*, \ell)}, \quad (8)$$

where  $\Gamma_{fus}$ ,  $\Gamma_{qf}$  and  $\Gamma_{sym}$  are corresponding widths determined by the level densities on the barriers  $B_{fus}^{(Z)*}(\alpha_i, \beta_i)$ ,  $B_{sym}^{*(Z)}(\alpha_i, \beta_i)$  and  $B_{qf}^{(Z)}(\alpha_i, \beta_i)$  are the intrinsic fusion, symmetric fission and quasifission barriers. To simplify the presentation of Eqs. (8), (9) and (10) the arguments  $(\alpha_i, \beta_i)$  of the functions  $E_Z^*(\alpha_i, \beta_i)$ ,  $T_Z(\alpha_i, \beta_i)$ ,  $B_{fus}^{(Z)*}$ ,  $B_{sym}^{*(Z)}$  and  $B_{qf}^{(Z)}$  are not indicated on their right sides of Eqs. (8), (9) and (10). The width  $\Gamma_i$  of the decay through the corresponding barriers  $B_i$  is determined by the level densities on the barriers [20]:

$$\Gamma_i^{(Z)}(B_i^{*(Z)}(\alpha_i, \beta_i), E_Z^*(\alpha_i, \beta_i), \ell) \approx \frac{\rho_i(E_Z^* - B_i^{*(Z)}, \ell)}{\rho_i(E_Z^*, \ell)} T_Z, \quad (9)$$

where a level density  $\rho(E_Z^*, \ell)$  is calculated by the expression [29]:

$$\rho(E_Z^*, \ell) = \left[ \frac{g^2}{g_1 g_2} \right]^{1/2} \frac{g}{6^{3/4} (2g E_Z^*)^{5/4}} \exp \left[ 2(a E_Z^*)^{1/2} \right], \quad (10)$$

where  $2g = g_1 + g_2$  and  $\pi^2 g_i / 6 = A_i / 11 \text{ MeV}^{-1}$ . The excitation energy  $E_Z^*(E_{c.m.}, \ell)$  of the DNS with the charge number  $Z$  of the light fragment is determined by the difference between collision energy  $E_{c.m.}$  and peculiarities of the driving potential  $U_{dr}$  calculated for the given value of  $\ell$ :

$$E_Z^*(E_{c.m.}, \ell, \alpha_i, \beta_i) = E_{c.m.} - V_{\min}(Z_P, A_P, R_m, \alpha_i, \beta_i) + \Delta U(Z, A, \ell, \alpha_i, \beta_i), \quad (11)$$

where

$$\Delta U(Z, A, \ell, \alpha_i, \beta_i) = U(Z_P, A_P, \ell, \alpha_i, \beta_i) - U(Z, A, \ell, \alpha_i, \beta_i) \quad (12)$$

is a change of the driving potential of the DNS during its evolution from the initial value:

$$U(Z_P, A_P, \ell, \alpha_i, \beta_i) = B_P(Z_P, A_P) + B_T(Z_T, A_T) - B_{CN} + V_{\min}(Z_P, A_P, \ell, \alpha_i, \beta_i) \quad (13)$$

to the final configuration with the charge and mass num-

bers  $Z$  and  $A$ , respectively:

$$U(Z, A, \ell, \alpha_i, \beta_i) = B_1(Z, A) + B_2(Z_{tot} - Z, A_{tot} - A) - B_{CN} + V_{min}((Z, A, \ell, \alpha_i, \beta_i). \quad (14)$$

When the final configuration of the DNS is compound nucleus Eq. 11 gives the CN excitation energy:

$$E_{CN}^*(E_{c.m.}, \ell) = E_{c.m.} + Q_{gg} - V_{CN}(\ell), \quad (15)$$

where  $Q_{gg} = B_1 + B_2 - B_{CN}$  is the energy balance of the reaction,  $B_1$ ,  $B_2$  and  $B_{CN}$  are the binding energies of the interacting nuclei and CN taken from the table in Ref. [30, 31];  $V_{CN}(\ell)$  is the CN rotational energy.

The shape of the colliding nuclei is included in consideration. Deformation parameters of the ground quadrupole and octupole states are taken from Ref. [31] of the reacting nuclei in this work while the ones of the first excited first  $2^+$  and  $3^-$  states are obtained from Refs. [32] and [33], respectively. The target nucleus  $^{248}\text{Cm}$  has a deformed shape in the ground state (see Table I) and possibilities of the collision with the different orientation angles  $\alpha_2$  relative to the beam direction are taken into account by averaging the contributions of collisions with different values of  $\alpha_2$ :

$$\langle \sigma_{fus}(E_{c.m.}, \beta_i^{(1)}, \ell) \rangle_{\alpha_2} = \int_0^{\pi/2} \sin \alpha_2 d\alpha_2 \times \sigma_i(E_{c.m.}, \ell; \beta_i^{(1)}, \alpha_2). \quad (16)$$

The projectile nucleus  $^{51}\text{V}$  is spherical in its ground state (see Table I) but the first excited quadrupole state  $\beta_{2+} = 0.2$  is considered as the zero-point vibrational state and  $\alpha_1$  is the direction of the spherical nucleus. For simplicity, we use  $\alpha_1 = 0$ . Consequently, a partial fusion cross section is found by averaging over values of the vibrational states  $\beta_2$  and  $\beta_3$  of the spherical nucleus:

$$\langle \sigma_{fus}(E_{c.m.}, \ell) \rangle_{\beta_i^{(1)}} = \int_{-\beta_{2+}}^{\beta_{2+}} d\beta_2 \int_{-\beta_{3-}}^{\beta_{3-}} d\beta_3 g(\beta_2, \beta_3) \times \sigma_{fus}(E_{c.m.}, \beta_{2+}^{(1)}, \beta_{3-}^{(1)}, \ell) \quad (17)$$

TABLE I. Deformation parameters  $\beta_2$  and  $\beta_3$  of the ground states and of the first excited  $2^+$  and  $3^-$  states of nuclei used in the calculations in this work.

Nucleus	$\beta_2$ [31]	$\beta_3$ [31]	$\beta_{2+}$ [32]	$\beta_{3-}$ [33]
$^{51}\text{V}$	0.0	0.0	0.2	0.17
$^{248}\text{Cm}$	0.235	0.0	0.297	0.065

The surface vibrations are regarded as independent harmonic vibrations and the nuclear radius is considered to be distributed as a Gaussian distribution [34],

$$g(\beta_2, \beta_3) = \exp \left[ -\frac{R_0^2 [\sum_{\lambda} \beta_{\lambda} Y_{\lambda 0}^*(\alpha_1)]^2}{2\sigma_{\beta}^2} \right] (2\pi\sigma_{\beta}^2)^{-1/2}. \quad (18)$$

$$\sigma_{\beta_2}^2 = \frac{R_0^2}{4\pi} \sum_{\lambda} \beta_{\lambda}^2. \quad (19)$$

The effect of the orientation angle of the axial symmetry axis on the complete fusion is seen from Fig. 1 where the dependence of the cross section of the CN formation in the  $^{51}\text{V} + ^{248}\text{Cm}$  reaction on the orientation angle of the axial symmetry axis of  $^{248}\text{Cm}$  relative to the beam direction and quadrupole deformation values  $\beta_{2+}$  at surface vibration is presented. The largest cross section of complete fusion corresponds to the orientation angles  $60 \div 70^\circ$  of the target nucleus.

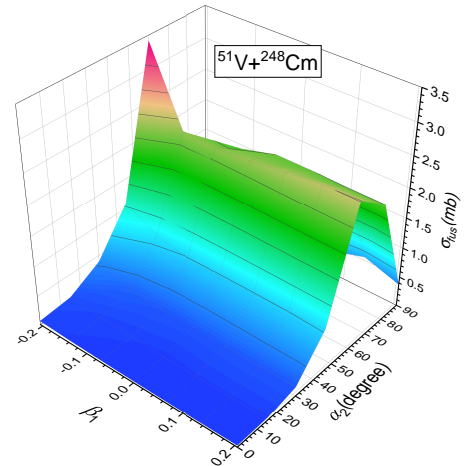


FIG. 1. The dependence of the cross section of the CN formation in the  $^{51}\text{V} + ^{248}\text{Cm}$  reaction on the orientation angle  $\alpha_2$  of the axial symmetry axis of  $^{248}\text{Cm}$  relative to the beam direction and quadrupole deformation values  $\beta_2$  at surface vibration of the  $^{51}\text{V}$  surface around spherical shape.

The reason of the increasing the cross section of complete fusion at the orientation angles  $60 \div 70^\circ$  of the target nucleus  $^{248}\text{Cm}$  is related with the decrease of the intrinsic fusion barrier  $B_{fus}^*$  at these values of  $\alpha_2$ . The values of the  $B_{fus}^*$  determined from the peculiarities of the driving potential are 10.67 and 6.20 MeV for orientation angles  $\alpha_2 = 30^\circ$  and  $60^\circ$ , respectively.

### C. Survival probability

The evaporation residue (ER) cross sections at the given value of the CN excitation energy  $E_x^*$  is calculated as a sum of the partial cross sections found for the angular momentum  $\ell$  of the system:

$$\sigma_{ER}^x(E_x^*) = \sum_0^{\ell_d} \sigma_{ER}^x(E_x^*, \ell), \quad (20)$$

where,  $\sigma_{ER}^x(E_x^*, \ell)$  describes the cross section of the particle emission from the intermediate nucleus with the excitation energy  $E_x^*$  at each step  $x$  of the de-excitation

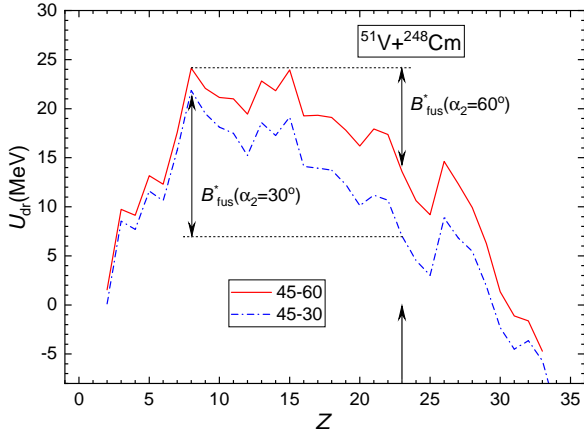


FIG. 2. The driving potential for the DNS formed in the  $^{51}\text{V}+^{248}\text{Cm}$  reaction calculated for the orientation angles  $30^\circ$  and  $60^\circ$  of the axial symmetry axis of  $^{248}\text{Cm}$  relative to the beam direction.

cascade by the formula [20, 35]:

$$\sigma_{ER}^x(E_x^*, \ell) = \sigma_{ER}^{x-1}(E_{x-1}^*, \ell) W_{\text{sur}}^x(E_{x-1}^*, \ell). \quad (21)$$

Here,  $\sigma_{ER}^{x-1}(E_{x-1}^*, \ell)$  is the partial cross section of the formation of the intermediate excited nucleus at the  $(x-1)$ th step, and obviously,

$$\sigma_{ER}^{(0)}(E_{CN}^*, \ell) = \langle \sigma_{\text{fus}}(E_{c.m.}, \ell) \rangle_{\beta_i^{(1)}}, \quad (22)$$

which is calculated by (16) and (17);  $W_{\text{sur}}^x(E_{x-1}^*, \ell)$  is the survival probability of the  $x$ th intermediate nucleus against fission along the de-excitation cascade of CN. The survival probability  $W_{\text{sur}}^x(E_{x-1}^*, \ell)$  is calculated by the statistical model implanted in KEWPIE2 [36], which is dedicated to the study of the evaporation residues at the synthesis of SHE.

The probability of the SHE depends on the competition between the fission and neutron evaporation which is determined by the survival probability  $W_{\text{sur}}^x(E_{x-1}^*, \ell)$ . It has been calculated by the statistical model [36], where Weisskopf approximation [37] is used to calculate neutron emission width:

$$\Gamma_n = \frac{(2S_n + 1)\mu_n}{\pi^2 \hbar^2} \int_0^{E_{CN}^* - B_n} \frac{\sigma_{inv}^n(\epsilon_n) \rho_B(E_B^*) \epsilon_n d\epsilon_n}{\rho_{CN}(E_{CN}^*)}, \quad (23)$$

where  $\rho_{CN}(E_{CN}^*)$  is the level density of the intermediate nucleus,  $E_B^*$  is the excitation energy of the residual nucleus after the emission of a neutron,  $B_n$  is the binding energy of the neutron with the residue nucleus,  $\mu_n = m_n(M_{CN} - m_n)/M_{CN}$  is the reduced mass of the system consisting of neutron and evaporation residue nucleus, where  $m_n$  and  $M_{CN}$  are masses of neutron and compound nucleus, respectively.  $S_n$  and  $\epsilon_n$  denote the

intrinsic spin of the neutron and its kinetic energy,  $\sigma_{inv}^n$  is the cross section for the time-reversed reaction.

In the KEWPIE2 code, the fission-decay width is estimated within the standard Bohr–Wheeler transition-state model [38]:

$$\Gamma_f^{BW} = \frac{1}{2\pi \rho_{CN}^{gs}(E_{CN}^*, J_{CN})} \int_0^{E_{CN}^* - B_f} \rho_C^{sd}(E_{sd}^*, J_{CN}) \times T_{\text{fiss}}(\epsilon_f) d\epsilon_f, \quad (24)$$

here, the excitation energy at the saddle point is equal  $E_{sd}^* = E_{CN}^* - B_f - \epsilon_f$ ,  $\rho_{CN}^{gs}(E_{CN}^*, J_{CN})$  and  $\rho_C^{sd}(E_{sd}^*, J_{CN})$  are the level densities of the nucleus at the ground-state and saddle-point deformation,  $J_{CN}$  is the total angular momentum of CN.

The KEWPIE2 code [36] utilizes the enhanced state-density equation, initially suggested in Ref.[39], to calculate different decay widths. The penetration factor,  $T_{\text{fiss}}(\epsilon_f)$ , corresponds to the Hill-Wheeler transmission coefficient [40]. The level-density parameter has been taken from the work which was recently proposed by Nerlo-Pomorska et al. [41]. In this work, the estimates for the level-density parameter obtained for different deformations are fitted by a liquid-drop type formula, which is expressed in the following form:

$$a = 0.092A + 0.036A^{2/3}\mathfrak{B}_s + 0.275A^{1/3}\mathfrak{B}_k - 0.00146 \frac{Z^2}{A^{1/3}} \mathfrak{B}_c, \quad (25)$$

where  $\mathfrak{B}_s$  is the surface term,  $\mathfrak{B}_k$  is the curvature term and  $\mathfrak{B}_c$  is the Coulomb term for a deformed nucleus [42].

It has been observed over the years that the influence of shell-correction effects on the level density parameter decreases as the excitation energy rises. To incorporate this damping effect, Ignatyuk's prescription [43] was used in the calculation, which considers the level density parameter to be dependent on the excitation energy. In the ground state, one has the following explicit expression:

$$a_{gs}(E^*) = a \left[ 1 + \left( 1 - e^{-E^*/E_d} \right) \frac{\Delta E_{sh}}{E^*} \right] \quad (26)$$

where the default value of the shell-damping energy  $E_d$  has been fixed at 19.0 MeV on the base of our previous calculations of the decay for the different reactions. The fission barrier consists of the macroscopic liquid-drop model and microscopic shell correction energy component [44]. The liquid-drop fission barrier is estimated by using the Lublin-Strasbourg Drop model [45]. The ground-state shell correction energies and the parameterizations for the liquid-drop fission barrier are using the mass table of Möller et al. [31].

### III. RESULTS AND DISCUSSIONS

The results of the total cross sections of the quasifission, complete fusion, and fast fission processes are pre-

sented in Fig. 3 by the red dashed, blue solid, and green dot-dashed curves, respectively. It is seen that quasifission is the dominant channel since the intrinsic barrier  $B_{\text{fus}}^*$  causing a hindrance to complete fusion is sufficiently large and quasifission barrier  $B_{\text{qf}}$  providing the stability of the DNS is small. Therefore, the fusion probability is small too.

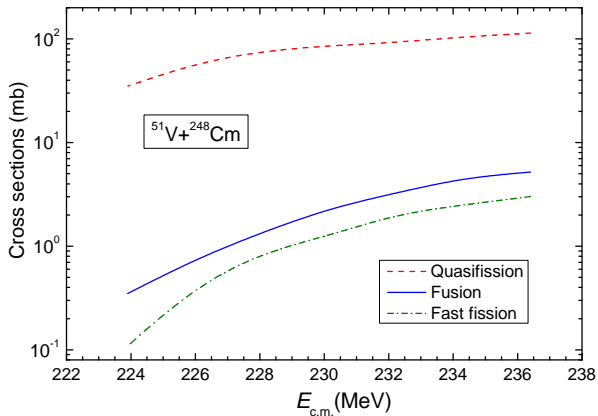


FIG. 3. Theoretical cross sections of the quasifission (red dashed curve), complete fusion (solid blue curve), and fast fission (dot-dashed green curve) for the  $^{51}\text{V}+^{248}\text{Cm}$  reaction as a function of  $E_{c.m.}$ .

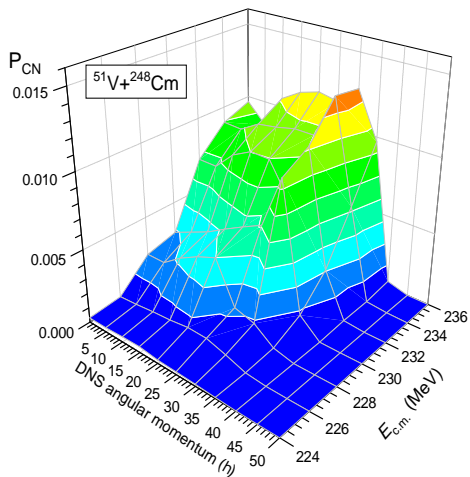


FIG. 4. Dependence of the fusion probability  $P_{\text{CN}}$  calculated for the  $^{51}\text{V}+^{248}\text{Cm}$  reaction as a function  $E_{c.m.}$  and angular momentum.

The dependence of the fusion probability on the orbital angular momentum and  $E_{c.m.}$  is seen in Fig. 4. It is calculated as a ratio of the partial cross section of the CN formation  $\sigma_{\text{fus}}^{(\ell)}$  to the partial capture cross section. The increase of the fusion probability by the increase of the beam energy since the DNS excitation energy  $E_Z^*$  increases at the fixed intrinsic fusion barrier  $B_{\text{fus}}^*$ . The de-

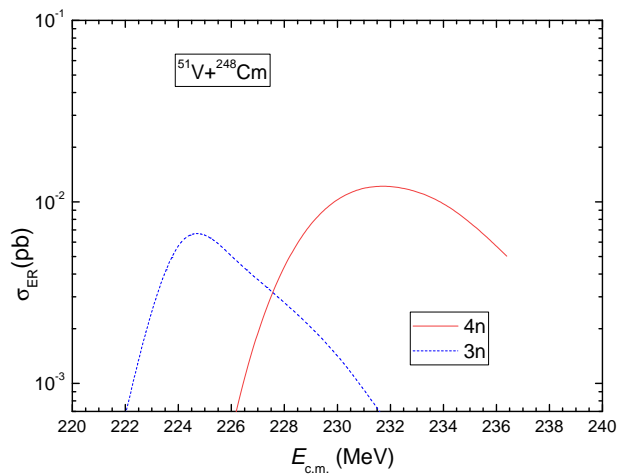


FIG. 5. Theoretical cross sections of the 3n (dashed blue curve) and 4n (solid red curve) channels of the ER formation in the  $^{51}\text{V}+^{248}\text{Cm}$  reaction as a function of  $E_{c.m.}$ .

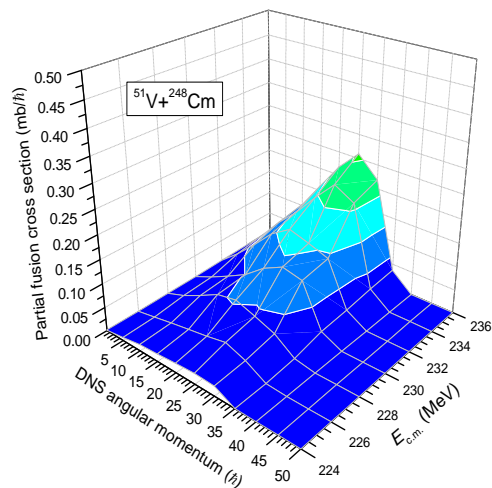


FIG. 6. The partial fusion cross sections calculated for the  $^{51}\text{V}+^{248}\text{Cm}$  reaction as a function of  $E_{c.m.}$  and orbital angular momentum.

crease of the  $P_{\text{CN}}$  by the increase of angular momentum  $L$  is explained by the increase of the  $B_{\text{fus}}^*$  and decrease of  $B_{\text{qf}}$  as a function of the angular momentum (see Table II). The increase of  $B_{\text{fus}}^*$  by the increase of  $L$  is related to the method of calculation of its values.  $B_{\text{fus}}^*$  is determined as a difference between the maximum value of the driving potential and its value corresponding to the charge and mass number of the colliding nuclei at the given value  $L$  (for the details see Refs. [20, 27]). Its maximum value corresponds to the ranges of the  $232 < E_{c.m.} < 236$  MeV and  $15 < L < 30\hbar$ . The excitation energy of the being formed compound nuclei is  $35 < E_{\text{CN}} < 39$  MeV. The results of the calculation of the ER cross section by the statistical method (KEWPIE2 code [36]) presented in Section II C are shown in Fig. 5. The maximum value of the exci-

tation function for the 4n channel is 12.3 fb ( $10^{-15}$  b) and it corresponds to the  $E_{CN} = 232$  MeV. The observation of the 3n channel is less probable since it is lower than 7 fb. In Table III, the results obtained in this work for the ER cross section in the 3n and 4n channels are compared with the corresponding predictions presented in Refs. [12, 17, 18, 46–48]. It is seen that our results are close to the predicted values of  $\sigma_{ER}$  in Refs. [12, 47].

One of the reasons the smallest value of the ER cross

TABLE II. Dependence of the intrinsic fusion  $B_{fus}^*$  and quasifission  $B_{qf}$  barriers of the entrance channel on the orbital angular momentum of collision  $L$ . The results are presented for the orientation angle of  $^{248}\text{Cm}$   $\alpha_2 = 60^\circ$  and  $\beta_2(1) = -0.12$ .

$L(\hbar)$	0	10	20	30	40	50
$B_{fus}^*$ (MeV)	11.46	11.48	12.70	14.12	36.32	48.70
$B_{qf}$ (MeV)	1.45	1.26	1.21	1.14	1.05	0.92

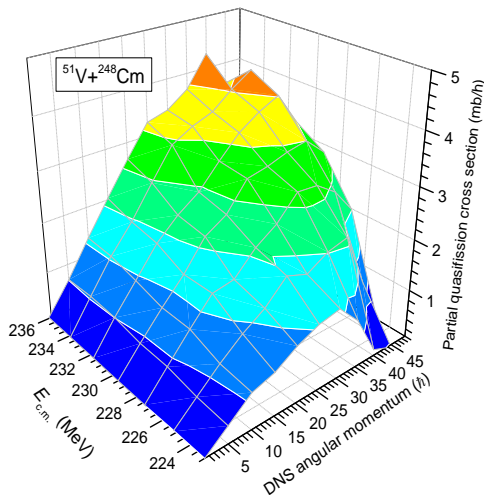


FIG. 7. The partial quasifission cross sections calculated for the  $^{51}\text{V}+^{248}\text{Cm}$  reaction as a function of  $E_{c.m.}$  and orbital angular momentum.

section is related to the small fusion cross section. The partial fusion cross sections presented in Fig. 6 show that the contribution of the collisions with the orbital angular momentum  $L = 15 \div 30\hbar$  at the collision energies  $E_{c.m.} = 232 \div 236$  is large. That means that the beam energy being used in the RIKEN experiments is optimal for the synthesis of the new superheavy element with charge number  $Z = 119$  [49]. The other reason for decreasing the number of synthesis events is the fast fission phenomenon which is the fission of the mono-nucleus survived against to quasifission process but could not reach the compound nucleus stage due to very value or absence of the fission barrier  $B_{CN}$  which is sensitive against its rotational energy and excitation energy. It is well known that the stability of superheavy elements is determined

exclusively by the shell effects of their nucleon structure. The dependence of the fast fission cross section on the orbital angular momentum and collision energy can be seen from Fig. 8. Its maximum values correspond to the collision energies as in the case of the complete fusion but fast fission is strong at the large values of the angular momentum  $L = 35 \div 45\hbar$ .

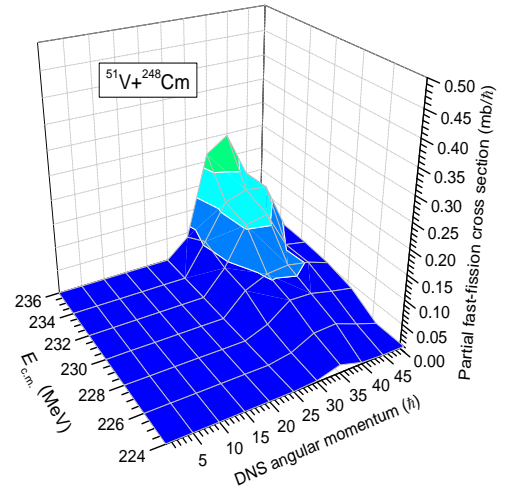


FIG. 8. The partial fast fission cross sections calculated for the  $^{51}\text{V}+^{248}\text{Cm}$  reaction as a function of  $E_{c.m.}$  and orbital angular momentum.

#### IV. CONCLUSIONS.

The ER cross section of 3n and 4n channels related to the synthesis of SHE of the charge number  $Z = 119$  in the  $^{51}\text{V}+^{248}\text{Cm}$  reaction has been calculated by the DNS model as a sum of the partial cross sections of the corresponding channels. The angular momentum distribution of the compound nucleus is estimated by the dynamical trajectory calculations of the capture probability which is considered as the DNS formation probability. The fusion probability decreases by the increase of the DNS angular momentum due to its influence on the intrinsic fusion barrier  $B_{fus}^*$ . The range  $\alpha_2 = 60^\circ \div 70^\circ$  of the orientation angle of the axial symmetry axis of the deformed target nucleus  $^{248}\text{Cm}$  is favorable for the formation of the compound nucleus. The fusion probability decreases at around  $\alpha_2 = 90^\circ$  since the number of the partial waves contributing to the capture decreases. Therefore, it is important to calculate the capture cross section dynamically. The 4n channel cross section of the SHE synthesis is larger than the 3n channel cross section maximum value of the ER cross section is 12.3 fb at  $E_{c.m.} = 232$  MeV.

TABLE III. Comparison of the theoretical predictions of the ER cross sections obtained in this work with results presented in Refs. [12, 17, 18, 46–48].

Reaction	$E_{c.m.}$ (MeV)	$3n$ (fb)	$E_{c.m.}$ (MeV)	$4n$ (fb)	Ref.
$^{51}\text{V}+^{248}\text{Cm}$	225	6.6	232	12.3	(this work)
	227	5.5	237	10.1	[12]
	228	2.9	236	5.9	[18]
	230	9.2	248	1.2	[17]
	232	19.5	245	99.6	[46]
	-	-	237	11.8	[47]
$^{50}\text{Ti}+^{249}\text{Bk}$	-	-	230	40	[47]
	-	-	230	18.7	[48]
	224	11.9	236	64	[12]
	226	48.2	244	5.67	[17]
	225	29.8	233	35.6	[18]
	-	-	-	-	-

- [1] S. Hofmann and G. Münzenberg, *Rev. Mod. Phys.* **72**, 733 (2000).
- [2] L. Stavsetra, K. E. Gregorich, J. Dvorak, P. A. Ellison, I. Dragojević, M. A. Garcia, and H. Nitsche, *Phys. Rev. Lett.* **103**, 132502 (2009).
- [3] Y. T. Oganessian, F. S. Abdullin, P. D. Bailey, D. E. Benker, M. E. Bennett, S. N. Dmitriev, J. G. Ezold, J. H. Hamilton, R. A. Henderson, M. G. Itkis, Y. V. Lobanov, A. N. Mezentsev, K. J. Moody, S. L. Nelson, A. N. Polyakov, C. E. Porter, A. V. Ramayya, F. D. Riley, J. B. Roberto, M. A. Ryabinin, K. P. Rykaczewski, R. N. Sagaidak, D. A. Shaughnessy, I. V. Shirokovsky, M. A. Stoyer, V. G. Subbotin, R. Sudowe, A. M. Sukhov, Y. S. Tsyganov, V. K. Utyonkov, A. A. Voinov, G. K. Vostokin, and P. A. Wilk, *Phys. Rev. Lett.* **104**, 142502 (2010).
- [4] C. E. Düllmann, M. Schädel, A. Yakushev, A. Türler, K. Eberhardt, J. V. Kratz, D. Ackermann, L.-L. Andersson, M. Block, W. Brüche, J. Dvorak, H. G. Essel, P. A. Ellison, J. Even, J. M. Gates, A. Gorshkov, R. Graeger, K. E. Gregorich, W. Hartmann, R.-D. Herzberg, F. P. Heßberger, D. Hild, A. Hübner, E. Jäger, J. Khuyagbaatar, B. Kindler, J. Krier, N. Kurz, S. Lahiri, D. Liebe, B. Lommel, M. Maiti, H. Nitsche, J. P. Omtvedt, E. Parr, D. Rudolph, J. Runke, B. Schausten, E. Schimpf, A. Semchenkov, J. Steiner, P. Thörle-Pospiech, J. Uusitalo, M. Wegrzecki, and N. Wiehl, *Phys. Rev. Lett.* **104**, 252701 (2010).
- [5] Y. T. Oganessian, F. S. Abdullin, S. N. Dmitriev, J. M. Gostic, J. H. Hamilton, R. A. Henderson, M. G. Itkis, K. J. Moody, A. N. Polyakov, A. V. Ramayya, J. B. Roberto, K. P. Rykaczewski, R. N. Sagaidak, D. A. Shaughnessy, I. V. Shirokovsky, M. A. Stoyer, N. J. Stoyer, V. G. Subbotin, A. M. Sukhov, Y. S. Tsyganov, V. K. Utyonkov, A. A. Voinov, and G. K. Vostokin, *Phys. Rev. C* **87**, 014302 (2013).
- [6] Y. T. Oganessian, F. S. Abdullin, C. Alexander, J. Binder, R. A. Boll, S. N. Dmitriev, J. Ezold, K. Felker, J. M. Gostic, R. K. Grzywacz, J. H. Hamilton, R. A. Henderson, M. G. Itkis, K. Miernik, D. Miller, K. J. Moody, A. N. Polyakov, A. V. Ramayya, J. B. Roberto, M. A. Ryabinin, K. P. Rykaczewski, R. N. Sagaidak, D. A. Shaughnessy, I. V. Shirokovsky, M. V. Shumeiko, M. A. Stoyer, N. J. Stoyer, V. G. Subbotin, A. M. Sukhov, Y. S. Tsyganov, V. K. Utyonkov, V. K. Utyonkov, A. A. Voinov, and G. K. Vostokin, *Phys. Rev. C* **87**, 054621 (2013).
- [7] J. Khuyagbaatar, A. Yakushev, C. E. Düllmann, D. Ackermann, L.-L. Andersson, M. Asai, M. Block, R. A. Boll, H. Brand, D. M. Cox, M. Dasgupta, X. Derkx, A. Di Nitto, K. Eberhardt, J. Even, M. Evers, C. Fahlander, U. Forsberg, J. M. Gates, N. Gharibyan, P. Golubev, K. E. Gregorich, J. H. Hamilton, W. Hartmann, R.-D. Herzberg, F. P. Heßberger, D. J. Hinde, J. Hoffmann, R. Hollinger, A. Hübner, E. Jäger, B. Kindler, J. V. Kratz, J. Krier, N. Kurz, M. Laatiaoui, S. Lahiri, R. Lang, B. Lommel, M. Maiti, K. Miernik, S. Minami, A. Mistry, C. Mokry, H. Nitsche, J. P. Omtvedt, G. K. Pang, P. Papadakis, D. Renisch, J. Roberto, D. Rudolph, J. Runke, K. P. Rykaczewski, L. G. Sarmiento, M. Schädel, B. Schausten, A. Semchenkov, D. A. Shaughnessy, P. Steinegger, J. Steiner, E. E. Tereshatov, P. Thörle-Pospiech, K. Tinschert, T. Torres De Heidenreich, N. Trautmann, A. Türler, J. Uusitalo, D. E. Ward, M. Wegrzecki, N. Wiehl, S. M. Van Cleve, and V. Yakusheva, *Phys. Rev. Lett.* **112**, 172501 (2014).
- [8] V. K. Utyonkov, N. T. Brewer, Y. T. Oganessian, K. P. Rykaczewski, F. S. Abdullin, S. N. Dmitriev, R. K. Grzywacz, M. G. Itkis, K. Miernik, A. N. Polyakov, J. B. Roberto, R. N. Sagaidak, I. V. Shirokovsky, M. V. Shumeiko, Y. S. Tsyganov, A. A. Voinov, V. G. Subbotin, A. M. Sukhov, A. V. Sabel'nikov, G. K. Vostokin, J. H. Hamilton, M. A. Stoyer, and S. Y. Strauss, *Phys. Rev. C* **92**, 034609 (2015).
- [9] J. Khuyagbaatar, A. Yakushev, C. E. Düllmann, D. Ackermann, L.-L. Andersson, M. Asai, M. Block, R. A. Boll, H. Brand, D. M. Cox, M. Dasgupta, X. Derkx, A. Di Nitto, K. Eberhardt, J. Even, M. Evers, C. Fahlander, U. Forsberg, J. M. Gates, N. Gharibyan, P. Golubev, K. E. Gregorich, J. H. Hamilton, W. Hartmann, R.-D. Herzberg, F. P. Heßberger, D. J. Hinde, J. Hoffmann, R. Hollinger, A. Hübner, E. Jäger, B. Kindler, J. V. Kratz, J. Krier, N. Kurz, M. Laatiaoui, S. Lahiri, R. Lang, B. Lommel, M. Maiti, K. Miernik, S. Minami, A. K. Mistry, C. Mokry, H. Nitsche, J. P. Omtvedt, G. K. Pang, P. Papadakis, D. Renisch, J. B.

- Roberto, D. Rudolph, J. Runke, K. P. Rykaczewski, L. G. Sarmiento, M. Schädel, B. Schausten, A. Semchenkov, D. A. Shaughnessy, P. Steinegger, J. Steiner, E. E. Tereshatov, P. Thörle-Pospiech, K. Tinschert, T. Torres De Heidenreich, N. Trautmann, A. Türler, J. Uusitalo, M. Wegrzecki, N. Wiehl, S. M. Van Cleve, and V. Yakusheva, *Phys. Rev. C* **102**, 064602 (2020).
- [10] S. Hofmann, S. Heinz, R. Mann, J. Maurer, G. Münzenberg, S. Antalic, W. Barth, H. G. Burkhard, L. Dahl, K. Eberhardt, R. Grzywacz, J. H. Hamilton, R. A. Henderson, J. M. Kenneally, B. Kindler, I. Kojouharov, R. Lang, B. Lommel, K. Miernik, D. Miller, K. J. Moody, K. Morita, K. Nishio, A. G. Popeko, J. B. Roberto, J. Runke, K. P. Rykaczewski, S. Saro, C. Scheidenberger, H. J. Schött, D. A. Shaughnessy, M. A. Stoyer, P. Thörle-Pospiech, K. Tinschert, N. Trautmann, J. Uusitalo, and A. V. Yeremin, *Eur. Phys. J. A* **52**, 180 (2016).
- [11] Y. T. Oganessian, V. K. Utyonkov, Y. V. Lobanov, F. S. Abdullin, A. N. Polyakov, R. N. Sagaidak, I. V. Shirokovsky, Y. S. Tsyganov, A. A. Voinov, A. N. Mezentsev, V. G. Subbotin, A. M. Sukhov, K. Subotic, V. I. Zagrebaev, S. N. Dmitriev, R. A. Henderson, K. J. Moody, J. M. Kenneally, J. H. Landrum, D. A. Shaughnessy, M. A. Stoyer, N. J. Stoyer, and P. A. Wilk, *Phys. Rev. C* **79**, 024603 (2009).
- [12] L. Zhu, W.-J. Xie, and F.-S. Zhang, *Phys. Rev. C* **89**, 024615 (2014).
- [13] F. Li, L. Zhu, Z.-H. Wu, X.-B. Yu, J. Su, and C.-C. Guo, *Phys. Rev. C* **98**, 014618 (2018).
- [14] X. J. Bao, Y. Gao, J. Q. Li, and H. F. Zhang, *Phys. Rev. C* **92**, 034612 (2015).
- [15] Z.-H. Liu and J.-D. Bao, *Phys. Rev. C* **87**, 034616 (2013).
- [16] J.-X. Li and H.-F. Zhang, *Phys. Rev. C* **105**, 054606 (2022).
- [17] X.-J. Lv, Z.-Y. Yue, W.-J. Zhao, and B. Wang, *Phys. Rev. C* **103**, 064616 (2021).
- [18] K. Siwek-Wilczyńska, T. Cap, and M. Kowal, *Phys. Rev. C* **99**, 054603 (2019).
- [19] B. M. Kayumov, O. K. Ganiev, A. K. Nasirov, and G. A. Yuldasheva, *Phys. Rev. C* **105**, 014618 (2022), [arXiv:2111.02861 \[nucl-th\]](https://arxiv.org/abs/2111.02861).
- [20] A. Nasirov, A. Fukushima, Y. Toyoshima, Y. Aritomo, A. Muminov, S. Kalandarov, and R. Utamuratov, *Nucl. Phys. A* **759**, 342 (2005).
- [21] A. J. Sierk, *Phys. Rev. C* **33**, 2039 (1986).
- [22] G. Adamian, N. Antonenko, and W. Scheid, *Nuclear Physics A* **678**, 24 (2000).
- [23] J. Hong, G. G. Adamian, and N. V. Antonenko, *Physics Letters B* **764**, 42 (2017).
- [24] G. Fazio, G. Giardina, A. Lamberto, R. Ruggeri, C. Saccà, R. Palamara, A. I. Muminov, A. K. Nasirov, U. T. Yakshiev, F. Hanappe, T. Materna, and L. Stuttgé, *J. Phys. Soc. Jpn.* **72**, 2509 (2003).
- [25] E. C. Kemble, *Phys. Rev.* **48**, 549 (1935).
- [26] K. Kim, Y. Kim, A. K. Nasirov, G. Mandaglio, and G. Giardina, *Phys. Rev. C* **91**, 064608 (2015).
- [27] G. Fazio, G. Giardina, G. Mandaglio, R. Ruggeri, A. I. Muminov, A. K. Nasirov, Y. T. Oganessian, A. G. Popeko, R. N. Sagaidak, A. V. Yeremin, S. Hofmann, F. Hanappe, and C. Stodel, *Phys. Rev. C* **72**, 064614 (2005).
- [28] H. Q. Zhang, C. L. Zhang, C. J. Lin, Z. H. Liu, F. Yang, A. K. Nasirov, G. Mandaglio, M. Manganaro, and G. Giardina, *Phys. Rev. C* **81**, 034611 (2010).
- [29] N. V. Antonenko, E. A. Cherepanov, A. K. Nasirov, V. P. Permjakov, and V. V. Volkov, *Phys. Rev. C* **51**, 2635 (1995).
- [30] G. Audi, A. Wapstra, and C. Thibault, *Nuclear Physics A* **729**, 337 (2003), the 2003 NUBASE and Atomic Mass Evaluations.
- [31] P. Moller, J. Nix, W. Myers, and W. Swiatecki, *Atomic Data and Nuclear Data Tables* **59**, 185 (1995).
- [32] S. Raman, C. Nestor, and P. Tikkanen, *Atomic Data and Nuclear Data Tables* **78**, 1 (2001).
- [33] R. Spear, *Atomic Data and Nuclear Data Tables* **42**, 55 (1989).
- [34] H. Esbensen, *Nuclear Physics A* **352**, 147 (1981).
- [35] G. Mandaglio, G. Giardina, A. K. Nasirov, and A. Sobiczewski, *Phys. Rev. C* **86**, 064607 (2012).
- [36] H. Lü, A. Marchix, Y. Abe, and D. Boilley, *Comput. Phys. Commun.* **200**, 381 (2016).
- [37] V. Weisskopf, *Phys. Rev.* **52**, 295 (1937).
- [38] N. Bohr and J. A. Wheeler, *Phys. Rev.* **56**, 426 (1939).
- [39] M. Grossjean and H. Feldmeier, *Nucl. Phys. A* **444**, 113 (1985).
- [40] D. L. Hill and J. A. Wheeler, *Phys. Rev.* **89**, 1102 (1953).
- [41] B. z. Nerlo-Pomorska, K. Pomorski, and J. Bartel, *Phys. Rev. C* **74**, 034327 (2006).
- [42] R. W. Hasse and W. D. Myers, *Geometrical Relationships of Macroscopic Nuclear Physics* (Springer Berlin, Heidelberg, 1988).
- [43] A. Ignatyuk, G. Smirenkin, and A. Tishin, *Sov. J. Nucl. Phys.* **21**, 485 (1975).
- [44] G. Giardina, G. Mandaglio, A. K. Nasirov, A. Anastasi, F. Curciarello, and G. Fazio, *Nucl. Phys. A* **970**, 169 (2018).
- [45] F. A. Ivanyuk and K. Pomorski, *Phys. Rev. C* **79**, 054327 (2009).
- [46] N. Ghahramany and A. Ansari, *Eur. Phys. J. A* **52**, 287 (2016).
- [47] G. G. Adamian, N. V. Antonenko, and H. Lenske, *Nuclear Physics A* **970**, 22 (2018).
- [48] G. G. Adamian, N. V. Antonenko, H. Lenske, and L. A. Malov, *Phys. Rev. C* **101**, 034301 (2020).
- [49] M. Tanaka, P. Brionnet, M. Du, J. Ezold, K. Felker, B. J. Gall, S. Go, R. K. Grzywacz, H. Haba, K. Hagino, S. Hogle, S. Ishizawa, D. Kaji, S. Kimura, T. T. King, Y. Komori, R. K. Lemon, M. G. Leonard, K. Morimoto, K. Morita, D. Nagae, N. Naito, T. Niwase, B. C. Rasco, J. B. Roberto, K. P. Rykaczewski, S. Sakaguchi, H. Sakai, Y. Shigekawa, D. W. Stracener, S. VanCleve, Y. Wang, K. Washiyama, and T. Yokokita, *Journal of the Physical Society of Japan* **91**, 084201 (2022), <https://doi.org/10.7566/JPSJ.91.084201>.